ChemPubSoc Europe

DOI: 10.1002/cctc.201500394

CHEMCATCHEM Full Papers

Enhanced CO Oxidation on the Oxide/Metal Interface: From Ultra-High Vacuum to Near-Atmospheric Pressures

Qiushi Pan,[a] Xuefei Weng,[a, b] Mingshu Chen,[b] Livia Giordano,[c] Gianfranco Pacchioni,[c] Claudine Noguera,[d, e] Jacek Goniakowski,*[d, e] Shamil Shaikhutdinov,*[a] and Hans-Joachim Freund[a]

We studied CO oxidation on FeO(111) films on Pt(111) at submonolayer oxide coverages at ultrahigh vacuum and near-atmospheric pressure conditions. The FeO(111) bilayer islands are inert towards CO_2 formation. In contrast, the FeO_{2-x} trilayer structure shows substantial CO_2 production that reaches a maximum at ≈40% coverage at both pressure conditions. The results provide compelling evidence that the FeO_{2-x}/Pt(111) interface is the most active in CO oxidation. Although FeO_{2-x} boundaries possesses weakly bound oxygen species, strong binding of CO to Pt favors the reaction at the FeO_{2-x}/Pt interface as compared to the FeO_{2-x}/FeO one, thus giving a rationale to the reactivity enhancement observed in systems exposing metal/oxide boundaries. In addition, oxygen diffusion from the interior of an FeO_{2-x} island to the active edge sites may be effective for the oxygen replenishment in the CO oxidation catalytic cycle.

Introduction

The catalytic oxidation of CO on metals is one of the most widely studied reactions in heterogeneous catalysis. To unravel the reaction mechanisms within the "surface science" approach, an enormous number of studies have been performed on model systems, primarily employing metal single crystal surfaces under ultrahigh vacuum (UHV) conditions. Recently, it has been recognized that ultrathin oxide films of transition metals grown on a metal support or those, natively formed on the noble metal surfaces under realistic pressure conditions, may show high activity, in particular at low temperatures, whereas "conventional" metal catalysts are, in essence, inert.[1] In attempts to find key factors which govern the reaction on such oxide films, a comparative study of CO oxidation over Fe, Mn, Zn, and Ru oxide ultrathin films at near-atmospheric pressures has been performed in our laboratories.[2] The results showed that oxygen binding energy in the oxide films, as measured by temperature-programmed desorption (TPD), plays the decisive role for the reaction: The more weakly bound surface oxygen species, the higher the reaction rate. Therefore, the oxygen-binding energy may serve as a good descriptor for oxidation reactions over thin films. It turned out, however, that the CO oxidation rate on ZnO monolayer films on Pt(111), which showed the least activity among the closed films, increases considerably at submonolayer (sub-ML) oxide coverage.[3] On the other hand, such a rate enhancement was not observed for the ZnO films supported on Ag(111).[4] The difference has been assigned to a much stronger CO adsorption on Pt(111) than on Ag(111) that increases the residence time for adsorbed CO and hence the probability to react with an oxygen supplied by ZnO.

The reactivity of ultrathin transition-metal oxide (TMO) films is closely related to so-called "strong metal–support interaction" (SMSI),[5] which is mostly discussed in terms of a full or partial encapsulation of metal particles by a thin oxide layer stemming from a support. In particular, our own studies of Pt nanoparticles deposited onto well-defined iron oxide surfaces showed the SMSI effect through encapsulation of the Pt surface by an iron oxide layer identified as FeO(111) monolayer film that readily grows on Pt(111) single crystal.[6,7] However, the FeO(111) film, initially stacked as an O–Fe bilayer, transforms at elevated oxygen pressures to an O-rich, FeO_{2-x} film with a trilayer (O–Fe–O) structural motif.[8] Although the film stoichiometry implies Fe cations in the formal oxidation state 4+, which is unusual for iron compounds, density functional theory (DFT) results showed that Fe ions in the trilayer structure are in the oxidation state 3+ owing to a substantial elec-

[a] Dr. Q. Pan, X. Weng, Dr. S. Shaikhutdinov, Prof. H.-J. Freund
Abteilung Chemische Physik
Fritz-Haber-Institut der Max-Planck-Gesellschaft
Faradayweg 4–6, 14195 Berlin (Germany)
E-mail: shaikhutdinov@fhi-berlin.mpg.de

[b] X. Weng, Prof. M. Chen
State Key Laboratory of Physical Chemistry of Solid Surfaces
South Siming Road 422, Xiamen, Fujian 361005 (P.R. China)

[c] Dr. L. Giordano, Prof. G. Pacchioni
Dipartimento di Scienza dei Materiali
Universitá di Milano-Bicocca
via Cozzi, 55-20125 Milano (Italy)

[d] Prof. C. Noguera, Dr. J. Goniakowski
CNRS, UMR 7588, Institut des Nanosciences de Paris
F-75005 Paris (France)
E-mail: Jacek.Goniakowski@insp.jussieu.fr

[e] Prof. C. Noguera, Dr. J. Goniakowski
Sorbonne Universités, UPMC Univ. Paris 06
UMR 7588, INSP
F-75005 Paris (France)

Supporting Information for this article is available on the WWW under http://dx.doi.org/10.1002/cctc.201500394.

tron transfer from the Pt(111) substrate. However, for brevity, we will use FeO and FeO_2 for the bilayer and trilayer structures, respectively.

The reaction mechanism of CO oxidation, addressed by DFT calculations using the model of a continuous FeO_2 film, suggested CO reacting with the weakly bound, topmost oxygen atom in the O–Fe–O trilayer, thus forming CO_2 that desorbs leaving an oxygen vacancy behind.[8a] The vacancy must be replenished by the reaction with molecular oxygen to end the catalytic cycle.

Recently, Bao and co-workers have addressed the reactivity of FeO(111) and other TMO(111) monolayer structures on Pt(111)[9] exposing the oxide/metal boundary. On the basis of DFT calculations,[9b,c] a Pt–cation ensemble was proposed, where coordinatively unsaturated TMO cations at the edges of TMO islands are highly active for O_2 adsorption and dissociation. Dissociated oxygen binds to Pt at the TMO/Pt interface and is responsible for the facile CO oxidation. The calculations employed a simplified model, using a TMO ribbon, which does not account for the experimentally observed epitaxial relationships of oxide and Pt and related lattice mismatches. Indeed, a very recent high-resolution scanning tunneling microscopy (STM) study[10] revealed several (up to five) types of edge structures of FeO(111) islands. To repeat this, the oxide phase was modeled by the bilayer, that is, O–TM–Pt(111), structure, which is not the structure relevant for technological CO oxidation reaction conditions, neither for FeO(111) nor for ZnO(0001) films on Pt(111).[3,8a] Following these studies, the highest reactivity on FeO(111)/Pt(111) must be obtained on the FeO_{1-x} islands, which are oxygen deficient at the rim and expose the unsaturated Fe cations. As a proof, in this[9c] and following-up publications,[9a,11] the authors provided a linear relationship obtained between the CO oxidation activity and the perimeter length only measured on the 0.25 ML FeO(111)/Pt(111) sample that underwent gradual oxide sintering upon stepwise annealing. The reaction rate was measured by monitoring the CO/Pt related signal in ultraviolet photoelectron spectra upon dosing of 5×10^{-8} mbar O_2 to the CO presaturated surface at room temperature. Although Bao's group confirmed the formation of FeO_2 trilayer islands upon oxidation of the "as grown" films at sub-monolayer coverages, they claim that these O-rich islands are inert.[11] The latter statement is at variance with our results, which clearly showed enhanced reactivity of the closed FeO_2 films. The discrepancy could, in principle, be linked to the differences in oxide preparation.[12] Indeed, Bao and co-workers found that UHV annealing at 573 K is sufficient to reduce FeO_2 back to FeO,[11] whereas the reduction only occurs at temperatures as high as 850 K in our films.[8a] On the other hand, the apparent controversy may be related to the reaction conditions and methods by which the reactivity was measured. While we monitor CO_2 production at near atmospheric pressures using a conventional batch reactor and gas chromatography, Bao's group used consumption of CO preadsorbed on Pt(111) by the molecular oxygen beam.

Recently, Huang and co-workers[13] have also studied the reactivity of FeO(111)/Pt(111) surfaces in the water gas shift reaction and preferential oxidation of CO in excess of H_2 using primarily TPD technique. It appears that the oxide structure is strongly affected by the reaction with water and hydrogen. A very recent DFT study,[14] performed on a more realistic model of FeO_x/Pt(111), showed that, beyond terraces of the oxygen-rich FeO_{2-x} phase, considered for a close film,[8a] also FeO_2/FeO and FeO_2/Pt boundaries may be involved in reactions. Finally, the metal–oxide synergy effect may also result from oxygen spillover from the oxide to the metal support.

In this work, we studied reactivity of FeO(111)/Pt(111) films at submonolayer coverage both in near atmospheric and UHV-compatible pressures to bridge the "pressure gap" that may cause some controversy in results obtained by different groups. Here we show that a much higher reactivity is, indeed, achieved by exposing an interface between the Pt support and the oxygen-rich FeO_{2-x} phase. Two synergetic effects concur: a low oxygen extraction energy at the FeO_2/Pt interface and a strong adsorption of CO on Pt(111) in its direct vicinity. Weak adsorption of CO on oxide surfaces levels out the (negligible) role of CO adsorption characteristics in the reaction over the closed oxide films, thus rendering the oxygen binding energy as the decisive parameter for reactivity of ultrathin oxide films.[2]

Results and Discussion

Experimental results

In Figure 1a, the kinetic curves obtained for CO oxidation over FeO(111)/Pt(111) films at 450 K in the reaction mixture of 10 mbar CO and 50 mbar O_2 (balanced by He to 1 bar) are

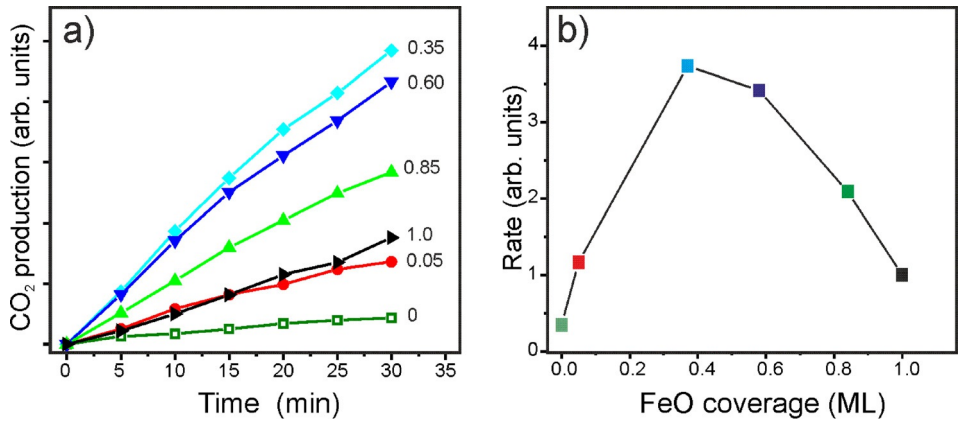

Figure 1. a) Kinetics of CO_2 production by CO oxidation over FeO(111) films grown on Pt(111) at the coverage as indicated. b) Reaction rate as a function of the FeO coverage. Reaction conditions: 10 mbar CO and 50 mbar O_2, balanced by He to 1 bar; 450 K.

shown for different oxide coverages. The integral amounts of CO_2 produced in reaction almost linearly grow in time indicating that the model catalysts do not suffer much from deactivation. CO titration of the open Pt sites in the spent catalysts by TPD showed essentially the same film coverage as in the "as-prepared" samples (not shown here). However, the corresponding oxygen desorption signal showed a strong peak at approximately 820 K (see details below), which is characteristic for the trilayer structure.[8a] These two findings suggest that in the course of reaction the initially grown FeO(111) islands transform into the FeO_{2-x} islands, which do not dewet under the O-rich reaction conditions, in agreement with STM results by Fu et al.[11]

The reaction rate versus film coverage plot (Figure 1b) clearly shows rate enhancement at sub-ML coverages reaching a maximum at approximately 0.4 ML. (We measured the rate at zero conversion to neglect any deactivation effects). The rate is substantially (by a factor of 3.5) higher than obtained for a closed, monolayer film, which is, in turn, more active than the pristine Pt(111) surface, in full agreement with our previous studies.[15] Clearly, the oxide/metal interface provides reaction sites more active than those on the (interior) surface of FeO_2 islands.

As oxygen binding energy was proposed as a good descriptor for reactivity of the closed ultrathin oxide films,[2] we first analyzed the observed rate enhancement in terms of weakly bonded oxygen which may be present at the rim of oxide islands. As previously, we used O_2 desorption temperature in TPD spectra as a measure of the oxygen binding strength. In Figure 2, the desorption traces of O_2 (32 amu) measured on the partially covered FeO(111)/Pt(111) films (in this case, ≈0.6 ML) exposed to 20 mbar of O_2 at 450 K are shown. The results for bare Pt(111) and a closed (i.e., 1 ML) film are shown, for comparison. Apparently, the sub-ML film exhibits desorption features of both, the Pt(111) support and the FeO_2 trilayer, although the spectrum cannot be presented as a superposition

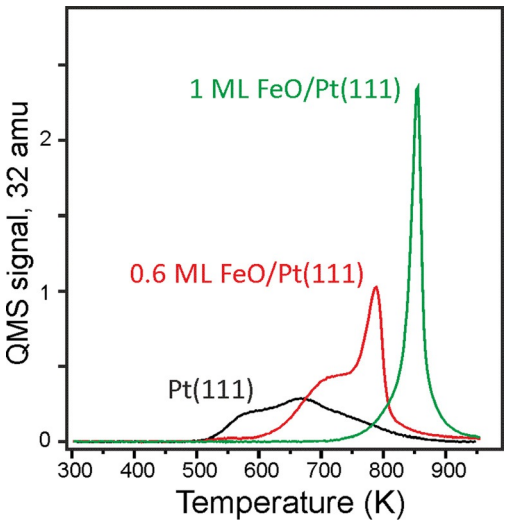

Figure 2. TPD spectra showing O_2 (32 amu) desorption signal upon heating the surfaces, as indicated, exposed to 20 mbar of O_2 at 450 K. Heating rate 3 K s^{-1}.

of individual signals from the two surfaces. A sharp signal at ≈800 K can straightforwardly be assigned to desorption from the FeO_2 phase, although the peak is at considerably lower temperature than observed for the closed film (≈850 K). Whether oxygen at the FeO/Pt interface exhibits characteristics different from bulk desorption is difficult to judge here because of its overlapping with oxygen desorption from uncovered Pt(111).

Nonetheless, solely on the basis of these O_2 TPD spectra one could suggest that the sub-ML oxide films are more active just because they provide more weakly bound oxygen species manifested itself by O_2 desorption at lower temperature than the closed film. On the other hand, following the same line of arguments, one should expect to see bare Pt(111) even more active because the oxygen desorbs from Pt(111) at lower temperatures. That is definitely not the case under the reaction conditions applied here (Figure 1). Basically, low activity of Pt(111) stems from the fact that strongly bonded CO blocks O_2 dissociation in the course of Langmuir–Hinshelwood mechanism. On the oxide surfaces, CO is thought to bind only weakly, thus leveling the role of CO in the reaction and making the oxygen bonding as a decisive parameter for reactivity of the closed oxide films.

To shed more light on the reaction mechanism for FeO(111)/Pt(111) films at sub-ML coverages, we conducted CO adsorption studies as a function of FeO coverage, exposure, and preparation conditions. The experiments were performed as follows. The FeO(111)/Pt(111) sample was exposed to 20 mbar O_2 at 450 K in the reactor and cooled to approximately 300 K before oxygen was pumped out to a pressure as low as 10^{-6} mbar. Then the sample was evacuated into UHV chamber and immediately cooled down to approximately 220 K prior to CO was adsorbed (typical exposure ≈1 L, 1 Langmuir = 1×10^{-6} Torr s), and TPD spectra were recorded by heating to 550 K. After the first TPD run, the sample was again cooled down and exposed to 1 L CO at 220 K, and the second TPD spectrum was measured. These adsorption/desorption cycles were repeated several times to monitor CO_2 production.

We first address the TPD results for bare Pt(111) (Figure 3a). The first CO exposure only resulted in the CO_2 signal (at ≈305 K) indicating that all adsorbed CO molecules reacted with oxygen to form CO_2. The CO_2 production was the highest in the second TPD run. Clearly, the reduced O coverage owing to the reaction with CO in the previous run allows more CO to adsorb and react. In the next runs, the CO_2 formation attenuates because of the lack of O atoms, and the CO signal converged to the one obtained on the clean Pt(111) surface. Oxygen consumption by the reaction with CO was monitored by recording 32 amu (O_2) signal (see Figure S1a in the Supporting Information), which on the bare surface exhibited a broad signal peaked at approximately 650 K and a prominent shoulder at approximately 560 K. The latter is associated either with ultrathin PtO_x overlayer or subsurface oxygen species, both formed only at high O_2 chemical potentials.[16] Regardless of its precise origin, this oxygen is found to be consumed first. However, the total amounts of CO_2 produced in repeated CO TPD spectra linearly correlate with the O_2 uptake (Figure S1b),

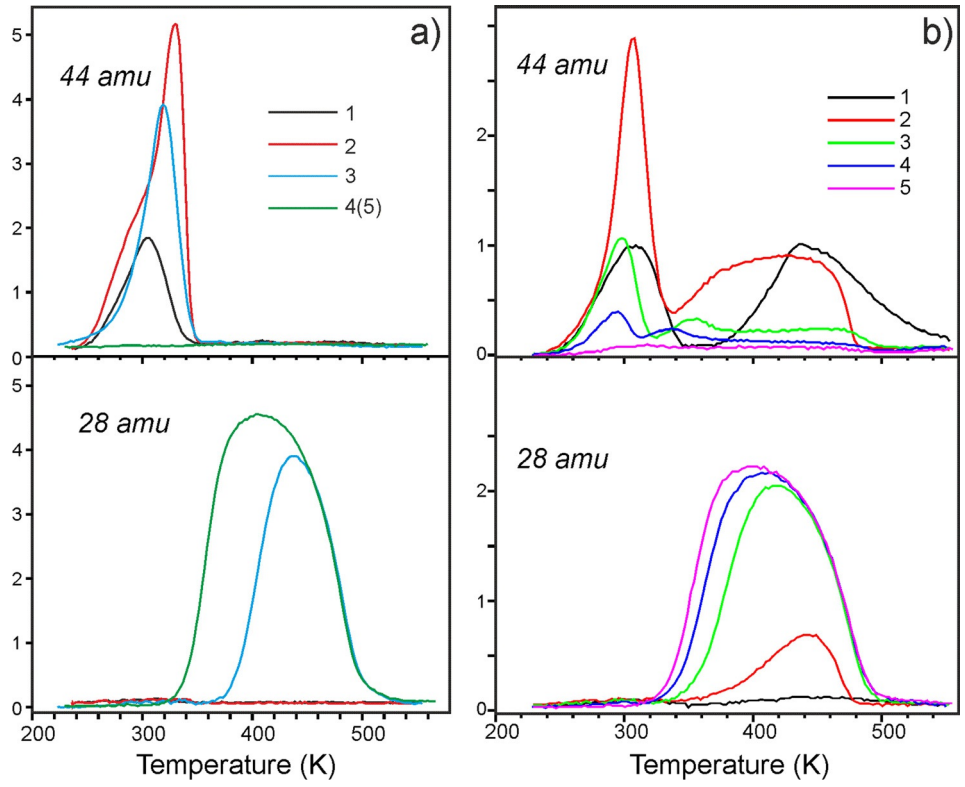

Figure 3. TPD spectra, showing CO_2 (44 amu) and CO (28 amu) signals, from a) the Pt(111) and b) the 0.6 ML FeO/Pt(111) samples, both pretreated in 20 mbar O_2 at 450 K for 10 min. The spectra were repeatedly measured *n* times, as indicated, and each time 1 L CO was adsorbed at ≈220 K. The heating rate was 3 K s^{-1}.

that is, independently on the nature of oxygen species. It, therefore, appears that the reaction first occurs between adsorbed CO and those surface O adatoms, which are more weakly bound because of its proximity to "oxidic" and/or subsurface oxygen species. The latter continuously replenishes the O atoms on the surface, which then react with CO in further TPD runs.

Before we address CO oxidation on the FeO(111) covered Pt(111) surface, we note that CO adsorption on the "as-grown" FeO(111) films did not result in any CO_2 production at any oxide coverage. If only the sub-ML films, following the film preparation at 1000 K (see Experimental Section), were cooled down to 300 K in 10^{-6} mbar of O_2, then CO_2 desorbing at approximately 300 K was observed in TPD spectra. However, the amounts of CO_2 reversely scaled with the FeO coverage (not shown), indicating that CO oxidation on the FeO(111)/Pt(111) surfaces only occurs on the oxide uncovered Pt(111) areas.

For comparison, Figure 3b shows the TPD results for an 0.6 ML FeO(111)/Pt(111) film first treated with O_2 at high pressures at the same conditions as used for bare Pt(111) presented in Figure 3a. Note that TPD spectra from a closed, that is, 1 ML, film did not detect any desorption signals, implying that CO does not adsorb on the FeO_2 terraces at these pressures (typically ≈10^{-6} mbar). On the sub-ML samples, no CO desorption other than obtained on Pt(111) is observed, thus suggesting that edges of the FeO_2 islands do not provide additional adsorption sites to CO. Moreover, after several CO adsorption/desorption cycles, the CO signal converged to the one observed on the same film prior to the high pressure O_2 treatment (see 28 amu spectra 4 and 5 in Figure 3b). In contrast to CO, CO_2 is produced in two well separated temperature regimes. The first one at low temperatures (LT), that is, approximately 300 K, is virtually identical to that obtained for Pt(111) (Figure 3a), and as such it is straightforwardly assigned to the reaction on open areas of Pt(111). CO_2 production at high temperatures (HT), that is, between 340 and 520 K, obviously missing on the bare Pt(111) surface, must be assigned to reactions on FeO_2/Pt(111) interface, as the closed film does not produce CO_2 at these conditions. The HT signal is the most intense in the first two TPD runs. Then it attenuates substantially, although one may recognize features at ≈360 K in the third and ≈340 K in the fourth runs. Interestingly, annealing to 1000 K during the fifth run did not reveal O_2 desorption at ≈800 K, which was initially present in the sample before CO adsorption (see Figure 2) and which is characteristic for the FeO_2 trilayer structure. Therefore, all weakly bonded oxygen species associated with the FeO_2 phase were ultimately consumed by the reaction with CO in these experiments.

The same experiments were then conducted for various oxide coverages. In Figure 4, the total amounts of CO_2 measured in five consecutive CO TPD spectra in the LT and HT regions, respectively, are plotted as a function of FeO(111) coverage in as-grown films. It is clear that the LT signal, in essence, reversely scales with the oxide coverage and as such it is assigned to reaction on uncovered areas of Pt(111). The observed linear relationship suggests no oxygen spillover from FeO_2 islands onto the Pt(111) surface. In contrast, CO_2 production in the HT state goes through the maximum in the same manner as observed for the CO oxidation rate at near atmospheric pressures (Figure 1b), both suggesting the reaction to occur on the interface between Pt(111) and FeO_2 trilayer.

In addition, we measured the amount of weakly bonded oxygen remained after CO adsorption experiments. The results also revealed the coverage effect: All samples at FeO coverages below 0.6 ML showed no more weakly bonded oxygen in the 32 amu (O_2) signal after the fifth CO TPD run, whereas the 0.85 ML sample revealed that only approximately 20% was consumed by the reaction with CO. To recall, the closed film did not manifest reaction with CO under these conditions. All

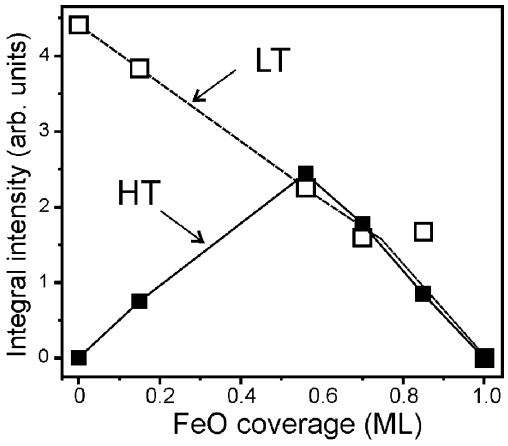

Figure 4. Total CO_2 production measured in LT and HT regions in five consecutive CO TPD runs (see Figure 3 for the 0.6 ML sample) as a function of FeO coverage.

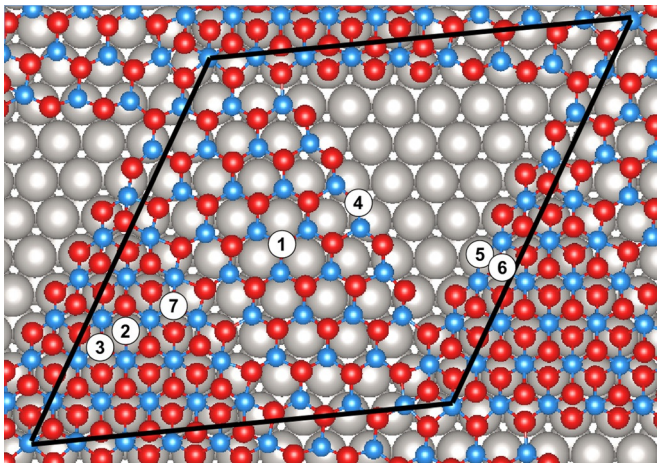

Figure 5. Computational model of a submonolayer FeO_x film on the Pt(111) surface. The nonequivalent oxygen sites are labeled 1–7: T-FeO (1), T_I-FeO_2 (2), T_S-FeO_2 (3), E-FeO/Pt (4), E_I-FeO_2/Pt (5), E_S-FeO_2/Pt (6), E-FeO_2/FeO (7). Pt, O, and Fe atoms are represented by gray, red, and blue spheres, respectively.

these findings indicate that oxygen reacting at the interface may be repopulated by oxygen from the interior parts of the FeO_2 islands during heating to 550 K and/or cooling down for the next CO adsorption. This may also explain the relatively broad HT signal and also some featuring (see, for example, peaks at ≈350 K for the 0.6 ML sample, see Figure 3 b), which may be caused by the simultaneous oxygen migration to the oxide rim on heating. Certainly, at high oxide coverages and large island sizes, oxygen consumption by CO reacting at oxide/metal interface is less pronounced than in the case of small islands.

Therefore, the combined experimental results provide compelling evidence that the enhanced reactivity observed for FeO partly covering the Pt(111) surface at realistic conditions is attributed to the reaction occurring at the rim of the FeO_2 islands formed at high oxygen pressures. Moreover, any reactions on the top of FeO_2 islands would be proportional to the oxide coverage, which is not the case. Whether the islands edges provide the most weakly bound oxygen and therefore become more readily reacting with an incoming CO molecule could not be judged solely by TPD. However, it seems more plausible that the oxide/metal interface is the most active simply because the CO molecules, involved in the reaction, adsorb on Pt sites in the proximity to the oxide. To end the catalytic cycle after CO_2 desorption, oxygen must be replenished. Bao and co-workers considering only the FeO bilayer model have previously suggested[9b] the replenishment to occur through O_2 dissociation at the coordinatively unsaturated Fe sites at the oxide edges. Although the FeO bilayer is certainly not the adequate one for reactions under realistic pressure conditions, we cannot exclude this scenario for the trilayer structure. However, our TPD results revealed that oxygen diffusion from the island interior to the edge sites may be operative as well.

Theoretical calculations

To shed more light on the reactivity of the FeO/Pt surfaces, we have performed DFT calculations to estimate the thermodynamic stability of oxygen at a variety of alternative terrace and boundary sites, characteristic of Pt-supported FeO_x film in sub-ML coverage. The computational model depicted in Figure 5 represents an oxide coverage of 0.6 ML, with an equal proportion of FeO and FeO_2, accounting for the case of large FeO_x islands on the Pt(111) surface. It consists of embedded FeO_2 islands, with trilayer O–Fe–O structure, located primarily in the region of the so-called "hcp" lattice registry (O ions on top of surface Pt atoms, Fe ions in the hollow sites), in which the oxygen-rich film forms the most easily.[8b] Conversely, bare FeO(111) is most stable in regions of "fcc" registry (both O and Fe ions in three-fold hollow sites of a Pt(111) substrate). The large unit cell contains also the region of a bare Pt(111) surface created by removing the oxide from regions of "top" registry (O ions in the hollow sites, Fe ions on top of a surface Pt), in which the stability of a FeO_x film is the lowest.[8b,17]

In the following, we focus on three different types of boundary sites, labeled E (edge): the oxide/oxide boundary (E-FeO_2/FeO) at the edge of the embedded FeO_2 islands, and oxide/metal boundaries at either FeO/Pt (E-FeO/Pt) or FeO_2/Pt (E-FeO_2/Pt) edge sites. Oxygen sites at FeO and FeO_2 terraces (T-FeO and T-FeO_2, respectively) and O adsorbed at Pt(111) will be used as a benchmark. In the case of FeO_2, oxygens in contact with vacuum, labeled S (surface), or in contact with Pt, labeled I (interface), will be systematically differentiated.

The calculated oxygen stability characteristics at the eight considered sites are summarized in Table 1. The vacancy formation energy ΔE shows a strong site dependence and ranges from nearly 3 eV for FeO terrace down to 1.3 eV for FeO_2/FeO boundary. We note that in this latter case ΔE is close to the calculated oxygen adsorption/desorption energy at the bare Pt(111) surface, which we find equal to 1.32 eV (obtained with one O in a (2×2) surface cell). While for each of the two oxide phases oxygen at boundary sites (E) is always less stable than at terraces (T), that is, consistent with the lower coordination of edge ions, oxygen extraction from FeO_2 requires less energy

Table 1. Calculated stability of oxygen at various sites of oxide submonolayer FeO_x/Pt as depicted in Figure 5. Oxygen extraction (vacancy formation) energy $\Delta E = E(FeO_x \text{ with an O vacancy}) + {}^1/_2\,E(O_2) - E(FeO_x)$ and corresponding desorption temperatures T_{max} (see text for details).

Site	ΔE [eV]	T_{max} [K]
T-FeO	2.93	1175
T_I-FeO_2	1.67	765
T_S-FeO_2	2.15	920
E-FeO/Pt	2.13	915
E_I-FeO_2/Pt	1.58	735
E_S-FeO_2/Pt	1.53	720
E-FeO_2/FeO	1.31	645

as compared to FeO. This is directly linked to the specificity of the FeO_2/Pt nanooxide, stabilized by a substantial electron transfer from the Pt(111) substrate, which enables anions to be fully reduced (formally O^{2-}) and cations to keep the Fe^{3+} oxidation state.[8,18] The lowest ΔE values are found at boundaries of embedded FeO_2 islands, either the oxide/metal (FeO_2/Pt) or the oxide/oxide (FeO_2/FeO) ones. Since upon oxygen extraction the electrons are back-transferred from FeO_2 to the Pt substrate and the tri-layer tends to (locally) recover the quasi-planar FeO-like structure, such recovery is, indeed, more easy at boundaries of the FeO_2 islands, where there are little or no structural constraints from neighboring atoms.[14]

Comparison with our previous results[8a,14] for the case of high oxide coverage reveals the sensitivity of oxygen extraction characteristics to the oxide coverage and to the local structure of the FeO_x/Pt interface. As expected, compared to Ref. [14], ΔE at T-FeO and T_I-FeO_2 are practically identical, showing a small effect of coverage for these terrace sites. Similarly, the present extraction energies at E-FeO/Pt and E-FeO_2/FeO sites differ by 5% only from those obtained for higher oxide coverage, and the difference is attributed to a somewhat different position of the oxide edges with respect to the Pt(111) lattice. In contrast, results obtained for T_S-FeO_2 and E-FeO_2/Pt sites are substantially different, with systematically larger oxygen extraction energies in the present 0.6 ML case. We note that such strong sensitivity to oxide coverage concerns uniquely oxygen of the oxygen-rich FeO_{2-x} phase. Basically, the electron exchange with the metal substrate and the resulting charging of the Pt(111) surface required for stabilization of the FeO_2 tri-layer makes the oxygen stability sensitive to the oxide coverage.

Calculated oxygen extraction energies can be linked to the experimental TPD data shown in Figure 2 with the help of Redhead analysis,[19] which links activation energy (E_{des}) and the temperature for desorption maximum (T_{max}): $E_{des}/RT^2_{max} = A/\beta \exp(-E_{des}/RT_{max})$, where R is the gas constant and β is the heating rate. Table 1 presents the computed values of T_{max} for the various oxygen sites, obtained with rate $\beta = 3\ K\,s^{-1}$ and the pre-exponential factor $A \approx 10^{13}\ s^{-1}$, commonly used for desorption of atoms and small molecules. We have assumed a linear relationship between desorption activation energy E_{des} and extraction energies ΔE: $E_{des} = a\Delta E + b$, $a = 0.93$ and $b = 0.55$ eV, adjusted so to reproduce the experimental desorption temperatures from a complete FeO(111)/Pt film (1190 K) and from a bare Pt(111) surface (650 K). The results prove that oxygen extracted from the embedded FeO_2 islands alone can be responsible for the main features of the observed oxygen desorption spectra in Figure 2. On the one hand, we find that desorption from FeO_2 terraces (T-FeO_2) occurs slightly below 800 K ($\Delta E = 1.67$ eV) that is, at a lower temperature than obtained for a monolayer coverage ($\approx$850 K[8a]), for which the calculated oxygen extraction energy ΔE is found to be 1.70 eV.[14] On the other hand, desorption from FeO_2/Pt boundaries may account for the feature observed at about 700 K as a shoulder to the main peak. We note also that the sensitivity of ΔE(FeO_2/Pt) to the oxide coverage discussed above is consistent with the relatively large width of the TPD feature. Finally, due to their close values for ΔE, contribution from FeO_2/FeO boundaries overlaps with the signal coming from oxygen on the bare Pt(111) surface.

While the oxygen extraction thermodynamics clearly identifies edge (E-FeO_2/Pt and E-FeO_2/FeO) sites as the most plausible candidates for CO oxidation (with a small preference for the latter), we complement the picture by an analysis of CO adsorption characteristics at these two boundaries.

As far as the FeO_2/Pt boundary is concerned (Figure 6a), our calculations in generalized gradient approximation (GGA) predict preferential CO adsorption at the neighboring hollow site

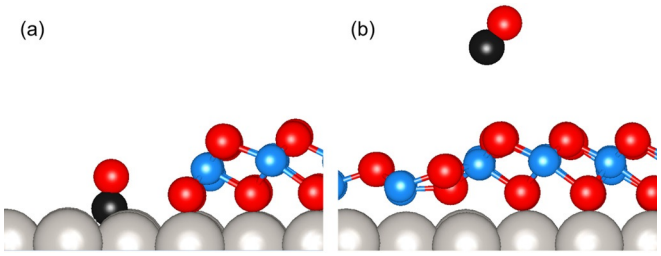

Figure 6. Most stable CO adsorption configurations at a) the FeO_2/Pt and b) FeO_2/FeO boundaries depicted in Figure 5. Pt, O, C, and Fe atoms are represented by gray, red, black, and blue spheres, respectively.

of the Pt(111) surface, with a large adsorption energy E_{ads}(FeO_2/Pt) = 2.05 eV. These adsorption characteristics are clearly reminiscent of those of a CO molecule on a bare Pt(111) surface, for which our present simulation predicts a somewhat stronger adsorption E_{ads}(Pt) = 2.19 eV (obtained with one CO molecule on a (2×2) surface cell). As a consequence, thermodynamics of both CO and O at the FeO_2/Pt boundary bears close similarity to their adsorption/desorption characteristics at the bare Pt(111) surface. However, the small reduction of CO–Pt bonding strength found in the direct vicinity of the FeO_2/Pt edge is expected to reduce the barrier for the $CO + O \rightarrow CO_2$ reaction. Not surprisingly, it also suggests a sensitivity of reaction thermodynamics and kinetics to the oxide coverage and precise metal-oxide registry, in line with the sensitivity of the oxygen extraction energies discussed above.

Conversely, CO adsorption at the FeO_2/FeO boundary (Figure 6b) is very weak, with an adsorption energy E_{ads}(FeO_2/FeO) = 0.05 eV. This value is only little higher than those obtained for FeO and FeO_2 terraces (0.03 eV and 0.01 eV, respectively, obtained for a single CO molecule on a (2×2) surface cell). It is noteworthy that, although van der Waals interactions (optB88-vdW[20]) increase the CO adsorption energy at terraces by about 0.1 eV, the effect is small, and it does not bring to a qualitative change to the stability of these weakly bound configurations. In any case, such small adsorption energies do not result in CO chemisorption to the oxide surface under the experimental conditions.

Whereas the strength of oxygen bonding at the FeO_2/Pt and FeO_2/FeO boundaries differs only little (1.5 eV vs. 1.3 eV), the very different characteristics of CO adsorption (2.05 eV vs. 0.05 eV) clearly indicates that these two sites have a different efficiency for CO oxidation. Indeed, since CO binds only weakly to the FeO_2/FeO boundary, the Eley–Rideal reaction mechanism is anticipated on these sites. Conversely, strong CO binding in the direct vicinity of the FeO_2/Pt boundaries makes the Langmuir–Hinshelwood mechanism operative. Although in the latter case CO and O binding characteristics are close to those obtained on the bare Pt(111) surface, the FeO_2 oxide phase provides O atoms which do not suffer from the CO blocking effect which, otherwise, poisons the CO oxidation reaction on the bare Pt surface.

Conclusions

The experimental results demonstrated much higher reactivity of FeO(111) films partly covering the Pt(111) surface than the closed films. Temperature-programmed desorption results showed that the "as-grown" FeO(111) bilayer islands are inert towards CO_2 formation. Only the FeO_{2-x} trilayer structures, which are formed at high oxygen pressures, showed substantial CO_2 production that reaches a maximum at approximately 40% coverage, that is, nearly the same as observed for the CO oxidation rate measured at near-atmospheric pressures. Corroborated by DFT calculations, the rate enhancement at submonolayer oxide coverages is assigned to the reaction at the oxide/metal boundary, between CO adsorbed on Pt(111) and oxygen at the edge sites of the FeO_2 trilayer islands. DFT-computed oxygen extraction characteristics clearly identify the boundaries of the FeO_2 phase as the preferential source of weakly bound oxygen. Although oxygen atoms are bound even more weakly at the FeO_2/FeO boundaries than to the FeO_2/Pt one, the reaction pathway is determined by their CO adsorption characteristics which differ substantially. CO adsorbs very weakly at FeO_2/FeO boundaries, thus leading to a less efficient Eley–Rideal type mechanism. Conversely, CO adsorption on Pt(111) in the vicinity to the FeO_2 island edges is as strong as on Pt(111), thus favoring a more efficient Langmuir-Hinshelwood mechanism. However, contrary to bare Pt(111), reaction at the FeO_2/Pt boundary is not affected by CO blocking the oxygen dissociation. In the course of catalytic reaction, the FeO_2 islands provide a reservoir of weakly bonded oxygen, which is continuously repopulated by oxygen dissociation and subsequent migration across the FeO_{2-x} islands to the active edge sites. As to better quantify the efficiency of the two reaction types, the calculations of the reaction pathway and associated activation barriers and their dependence on the oxide coverage and metal-oxide registry are currently in progress.

Certainly, for the rate enhancement to occur CO must adsorb sufficiently strongly, otherwise it desorbs intact before reaction with oxygen. Therefore, weakly adsorbing metal surfaces, such as Ag(111), do not show such effect as previously reported for ZnO(0001) films.[4] Accordingly, using oxygen bonding energy as a principal descriptor for CO oxidation over ultrathin oxide films seems to be valid only for the systems exhibiting relatively weak CO adsorption which does not compete for oxygen adsorption sites. In the case of systems exposing a metal/oxide interface, the reactivity may be considerably enhanced by metals strongly adsorbing CO like Pt. In such cases, the model of overlapping states[21] seems to be fairly predictive, suggesting high activity when the desorption profiles for each individual molecule reacting at the surface overlap.

Experimental Section

Experimental methods

The experiments were performed in an UHV chamber (base pressure below 2×10^{-10} mbar) equipped with low-energy electron diffraction (LEED), Auger electron spectroscopy (AES), and quadrupole mass-spectrometer (QMS, from Hiden) for TPD measurements. The Pt(111) single crystal was spot-welded to thin Ta wires for resistive heating. The crystal was cleaned using repeated cycles of Ar^+ bombardment and annealing in UHV at ≈1200 K. Residual carbon was removed by oxidation at ≈900 K in 10^{-6} mbar of O_2. Cleanliness of the crystal was checked by LEED, AES, and CO TPD prior to each preparation of the FeO(111) films. The films were grown on Pt(111) kept at 300 K by Fe vapor deposition from a Fe rod (99.99%, from Goodfellow) using commercial e-beam assisted evaporator (Focus EMT3), followed by annealing in 10^{-6} mbar of O_2 at 1000 K for 2 min. The chamber houses a high-pressure reaction cell for reactivity studies at atmospheric pressures using a gas chromatograph (from Agilent) for the gas composition analysis. The reaction mixture (10 mbar CO and 50 mbar O_2, balanced by He to 1 bar) was dosed at room temperature and circulated with a membrane pump for 20 min to reach constant flow. Then the sample was heated to the reaction temperature 450 K with a rate 1 Ks^{-1}. After reaction the sample was cooled down to room temperature while the cell was pumped out down to ≈10^{-6} mbar before it was evacuated for surface characterization.

Computational methods

All DFT calculations were performed with the Vienna Ab-initio Simulation Package (VASP),[22] using Projector Augmented Wave (PAW) method[23] to represent the electron–core interaction, and the Perdew-Wang 91 (PW91)[24] gradient-corrected exchange–correlation functional. Following our previous stud-

ies,[17] iron oxides were treated with the DFT+U approach in the form proposed by Dudarev,[25] with U_{Fe}–J_{Fe} = 3 eV. FeO_x/Pt(111) system was represented by a three-layer-thick Pt(111) slab with the FeO_x oxide adsorbed on one side only. The two bottom Pt layers were hold fixed while the surface Pt layer and the oxide film were fully relaxed (threshold on forces equal to 0.01 eV Å^{-1}). The slabs were separated by at least 10 Å of vacuum and the so-called dipole corrections were applied in order to eliminate the residual dipoles in the direction perpendicular to the surface. To take into account the effect of lattice mismatch between the Pt(111) substrate and the FeO_x oxide layer and to mimic the coincidence structures observed experimentally,[26] a $(\sqrt{73}\times\sqrt{73})$R5.8°–FeO(111)//$(\sqrt{91}\times\sqrt{91})$R5.2°–Pt(111) periodic supercell has been used. It contains 415 atoms per unit cell, making Γ point sufficient to sample the Brillouin zone. In all calculations, we have used soft oxygen and carbon pseudopotentials (energy cutoff of 280 eV)[27] and imposed a row-wise anti-ferromagnetic alignment of Fe spins.[17]

Acknowledgements

The authors from FHI acknowledge Cluster of Excellence UNICAT administered by TU Berlin, and SFB 1109 administered by HU Berlin, and Fonds der Chemischen Industrie for financial support. X.W. thanks China Scholarship Council for the fellowship. The work of LG and GP was supported by the FIRB Project RBAP115AYN "Oxides at the nanoscale: multifunctionality and applications". The authors acknowledge the COST Action CM1104.

Keywords: interfaces · iron · monolayer · oxidation · platinum

[1] S. Shaikhutdinov, H.-J. Freund, *Annu. Rev. Phys. Chem.* **2012**, *63*, 619–633.
[2] Y. Martynova, S. Shaikhutdinov, H.-J. Freund, *ChemCatChem* **2013**, *5*, 2162–2166.
[3] Y. Martynova, B. H. Liu, M. E. McBriarty, I. M. N. Groot, M. J. Bedzyk, S. Shaikhutdinov, H. J. Freund, *J. Catal.* **2013**, *301*, 227–232.
[4] Q. Pan, B. H. Liu, M. E. McBriarty, Y. Martynova, I. M. N. Groot, S. Wang, M. J. Bedzyk, S. Shaikhutdinov, H. J. Freund, *Catal. Lett.* **2014**, *144*, 648–655.
[5] S. J. Tauster, *Acc. Chem. Res.* **1987**, *20*, 389–394.
[6] a) M. Lewandowski, Y. N. Sun, Z. H. Qin, S. Shaikhutdinov, H. J. Freund, *Appl. Catal. A* **2011**, *391*, 407–410; b) M. G. Willinger, W. Zhang, O. Bondarchuk, S. Shaikhutdinov, H.-J. Freund, R. Schlögl, *Angew. Chem. Int. Ed.* **2014**, *53*, 5998–6001; *Angew. Chem.* **2014**, *126*, 6108–6112.
[7] G. H. Vurens, M. Salmeron, G. A. Somorjai, *Surf. Sci.* **1988**, *201*, 129–144.
[8] a) Y.-N. Sun, L. Giordano, J. Goniakowski, M. Lewandowski, Z.-H. Qin, C. Noguera, S. Shaikhutdinov, G. Pacchioni, H.-J. Freund, *Angew. Chem. Int. Ed.* **2010**, *49*, 4418–4421; *Angew. Chem.* **2010**, *122*, 4520–4523; b) L. Giordano, M. Lewandowski, I. M. N. Groot, Y. N. Sun, J. Goniakowski, C. Noguera, S. Shaikhutdinov, G. Pacchioni, H. J. Freund, *J. Phys. Chem. C* **2010**, *114*, 21504–21509.
[9] a) Q. Fu, F. Yang, X. Bao, *Acc. Chem. Res.* **2013**, *46*, 1692–1701; b) D. Sun, X.-K. Gu, R. Ouyang, H.-Y. Su, Q. Fu, X. Bao, W.-X. Li, *J. Phys. Chem. C* **2012**, *116*, 7491–7498; c) Q. Fu, W.-X. Li, Y. Yao, H. Liu, H.-Y. Su, D. Ma, X.-K. Gu, L. Chen, Z. Wang, H. Zhang, B. Wang, X. Bao, *Science* **2010**, *328*, 1141–1144.
[10] H. Zeuthen, W. Kudernatsch, L. R. Merte, L. K. Ono, L. Lammich, F. Besenbacher, S. Wendt, *ACS Nano* **2015**, *9*, 573–583.
[11] Q. Fu, Y. Yao, X. Guo, M. Wei, Y. Ning, H. Liu, F. Yang, Z. Liu, X. Bao, *Phys. Chem. Chem. Phys.* **2013**, *15*, 14708–14714.
[12] Y. Yao, Q. Fu, Z. Wang, D. Tan, X. Bao, *J. Phys. Chem. C* **2010**, *114*, 17069–17079.
[13] L. Xu, Z. Wu, Y. Jin, Y. Ma, W. Huang, *Phys. Chem. Chem. Phys.* **2013**, *15*, 12068–12074.
[14] L. Giordano, G. Pacchioni, C. Noguera, J. Goniakowski, *ChemCatChem* **2014**, *6*, 185–190.
[15] Y. N. Sun, Z. H. Qin, M. Lewandowski, E. Carrasco, M. Sterrer, S. Shaikhutdinov, H. J. Freund, *J. Catal.* **2009**, *266*, 359–368.
[16] a) D. Bashlakov, L. F. Juurlink, M. M. Koper, A. Yanson, *Catal. Lett.* **2012**, *142*, 1–6; b) H. Steininger, S. Lehwald, H. Ibach, *Surf. Sci.* **1982**, *123*, 1–17; c) J. L. Gland, B. A. Sexton, G. B. Fisher, *Surf. Sci.* **1980**, *95*, 587–602; d) N. R. Avery, *Chem. Phys. Lett.* **1983**, *96*, 371–373.
[17] L. Giordano, G. Pacchioni, J. Goniakowski, N. Nilius, E. D. L. Rienks, H.-J. Freund, *Phys. Rev. B* **2007**, *76*, 075416.
[18] L. Giordano, G. Pacchioni, C. Noguera, J. Goniakowski, *Top. Catal.* **2013**, *56*, 1074–1081.
[19] P. A. Redhead, *Vacuum* **1962**, *12*, 203–211.
[20] a) M. Dion, H. Rydberg, E. Schröder, D. C. Langreth, B. I. Lundqvist, *Phys. Rev. Lett.* **2004**, *92*, 246401; b) J. Klimeš, D. R. Bowler, A. Michaelides, *Phys. Rev. B* **2011**, *83*, 195131; c) K. J. Klimes, D. R. Bowler, A. Michaelidis, *J. Phys. Condens. Matter* **2010**, *22*, 022201.
[21] A. M. Doyle, S. K. Shaikhutdinov, H. J. Freund, *J. Catal.* **2004**, *223*, 444–453.
[22] G. Kresse, J. Furthmüller, *Phys. Rev. B* **1996**, *54*, 11169–11186.
[23] G. Kresse, D. Joubert, *Phys. Rev. B* **1999**, *59*, 1758–1775.
[24] J. P. Perdew, J. A. Chevary, S. H. Vosko, K. A. Jackson, M. R. Pederson, D. J. Singh, C. Fiolhais, *Phys. Rev. B* **1992**, *46*, 6671–6687.
[25] S. L. Dudarev, G. A. Botton, S. Y. Savrasov, C. J. Humphreys, A. P. Sutton, *Phys. Rev. B* **1998**, *57*, 1505–1509.
[26] M. Ritter, W. Ranke, W. Weiss, *Phys. Rev. B* **1998**, *57*, 7240–7251.
[27] W. Zhang, Z. Li, Y. Luo, J. Yang, *J. Phys. Chem. C* **2009**, *113*, 8302–8305.

Received: April 9, 2015
Revised: June 10, 2015
Published online on August 11, 2015